The Corrosion of Materials in Spallation Neutron Sources

R. Scott Lillard, Darryl P. Butt
Materials Corrosion and Environmental Effects Lab
Materials Science and Technology Division, MST-6
Los Alamos National Laboratory
Los Alamos New Mexico 87545

Summary

This paper presents a summary of our current efforts to measure the real-time corrosion rates of Alloy 718 (718) during 800 MeV proton radiation at currents up to 1 mA. Specially designed corrosion probes, which incorporated ceramic seals, were mounted in a water manifold that allowed samples to be directly exposed to the proton beam at the Los Alamos Neutron Science Center. The water system that supplied the manifold provided a means for controlling water chemistry, measuring dissolved hydrogen concentration, and measuring the effects of water radiolysis and water quality on corrosion rate. Real-time corrosion rate measurements during proton irradiation showed an exponential increase in corrosion rate with proton beam current. These results are discussed within the context of water radiolysis at the diffusion boundary layer / beam-spot interface. However, additional factors that may influence these parameters, such as oxide spallation and charge build-up in the passive film, are not ruled out. Results from a 718 sample placed in the water system downstream from the beam spot are also presented.

Introduction to Spallation Neutron Sources

Over the course of the past 30 years numerous particle accelerators have been developed around the world: the Fermi proton/anti proton ring in Illinois, the KEK proton synchrotron in Japan, the CERN proton synchrotron in France, and the ISIS pulsed neutron spallation source in Oxford to name a few. The world's highest power spallation neutron source is the Los Alamos Neutron Science Center (LANSCE) at Los Alamos National Laboratory. At LANSCE, 800 MeV protons at currents as high as 1 mA strike a tungsten target producing high energy neutrons. Circulating water loops are used to cool the target and to moderate the energy of the neutrons. This source of moderated neutrons is then used for neutron scattering and neutron diffraction studies.

It has also been proposed that spallation neutrons may be used to produce tritium. This has led to the Accelerator Production of Tritium (APT) project headed by the Los Alamos National Laboratory in collaboration with Westinghouse Savannah River Company, Brookhaven National Laboratory, Lawrence Livermore National Laboratory and Sandia National Laboratories. In APT, high energy protons would be accelerated to 1.7 GeV by a linac operating at currents over 1 mA. As at LANSCE, high energy neutrons would be produced when the proton beam leaves ultra-high vacuum and strikes a tungsten target. A circulating water loop would provide neutron moderation and target cooling. Tritium would be produced by "capturing" the moderated neutrons in an ^{3}He gas blanket. To study the feasibility of building such a facility, the APT project has been divided into three separate thrust areas 1) Accelerator Technology (RF quadropole design, high energy linac, etc.), 2) Target/Blanket Technology (neutron production and materials verification), and 3) Tritium Separation Technology (^{3}He blanket, isotope separation, etc.) The materials verification studies for the target blanket loop include examining the effects of proton / neutron radiation on materials strength and ductility as well as materials corrosion during high energy proton irradiation and in radiolyzed water. This paper presents a summary of our current efforts to measure the real-time corrosion rates of Alloy 718 (718) during high energy proton irradiation at LANSCE.

Radiation and Radiolysis Effects on Corrosion

The irradiation of water by ionizing radiation (electron, proton, gamma, etc.) results in the deposition of energy along tracks. This energy deposition results in nonhomogenous reactions that produce a variety of intermediate and stable water radiolysis products, such as: H_2, O_2, H_2O_2, OH, H, e^-_{aq}, HO_2, O_2^-, HO_2^-, OH^-, H^+ (1, 2, 3, 4, 5, 6). The lifetime of many of these species is short, on the order of microseconds or less. While short-lived water radiolysis products may be an important consideration in the corrosion mechanism of materials exposed directly to ionizing radiation (as the short lived species will be formed at the metal / solution / radiation interface) they will have little impact on materials "downstream" from the radiation source in a cooling water loop. The corrosion reaction mechanism of the downstream materials will most likely be controlled by long-lived radiolysis products such as hydrogen peroxide (H_2O_2) and oxygen (O_2) as well as contaminants and spallation products. Oxidizing water radiolysis products such as H_2O_2 and O_2 are detrimental as corrosion reactions are generally cathodically limited. That is, anodic (oxidation) and cathodic (reduction) reactions at the rest potential are at steady state (i.e., you can not store charge) and the rate determining step is typically the cathodic reaction. Therefore, an increase in the concentration of the oxidizing species increases the rate determining step in the corrosion reaction and, correspondingly, increases the anodic reaction rate. To minimize the concentration of total oxidant in solution due to gamma (γ) radiolysis, boiling water reactors and pressurized water reactors (BWR and PWR respectively) have employed a method known as hydrogen water chemistry (HWC) (7, 8, 9, 10, 11, 12).

While numerous studies have focused on the effects of gamma radiation and radiolysis on corrosion rate, little attention has been given to the effects of proton radiation. Simnad and Smoluchowski measured the real-time open circuit potential (OCP) of a tungsten target during irradiation in a 260 MeV proton beam(13). They found that the OCP of the tungsten target became more positive with increasing proton fluences. Their interpretation of this result was that particle radiation created defects at the metal surface which contributed to the observed electrode potential increase. They theorize that the defects had to be large (dislocation lines, loops, or collapsed

vacancy clusters) because isolated vacancies and interstitials would presumably disappear rapidly given their proximity to the surface. Simnad and Smoluchowski also investigated the effects of proton radiation on the dissolution rate iron(14). In these experiments weight loss measurements found, for a fluence of $1x10^{16}$ protons/cm^2, that the dissolution of iron increased from 0.4 mg/cm^2 in the absence of irradiation to approximately 1.4 mg/cm^2 during irradiation. In similar studies during γ irradiation, real-time increases in the OCP and corrosion rate have been observed for 304L and 316L(15), aluminum alloys(16), and grade 12 titanium(17, 18) samples. It was demonstrated in each of these studies that increases in the OCP and corrosion rate may be attributed to an increase in concentration of total oxidant in solution.

Design of the LANSCE Experiments

All experiments were conducted at the A6 Target Station which is located in Experimental Area A just in front of the linac beam stop at LANSCE. At this station the proton beam had a Gaussian distribution of 2σ = 3 cm and an energy of 800 MeV. The beam had a characteristic macropulse repetition rate between 10 and 100 Hz and a gate length of 625 to 835 microseconds. Beam currents were controlled by varying the repetition rate and the number of micropulses in the gate and, therefore, the gate length. Nominally, the currents varied between 1 and 400 μA. A detailed description of the beam profile as well as diagrams of the beam at A6 has been presented elsewhere(19). The corrosion water loop (Figure 1) at the A6 Target Station consisted of a pumping system to control flow and pressure to the manifold which held the corrosion samples in-beam.

To measure the real-time in-beam corrosion rate of a material as a function of beam current and time, it was necessary to electrically isolate the corrosion samples from the stainless steel 304 water system. Conventionally, this can be accomplished with commercially available corrosion probes that use metal-to-glass seals. However, in addition to physical damage proton irradiation of glass causes its conductivity to become unacceptably high, rendering the seal useless. Therefore, an alternate sealing method was chosen. As shown in Figure 2, the in-beam corrosion

samples were metal tubes (one end closed, one end open) with an outside diameter of 1.27 cm and a length of 15.87 cm. The wall thickness was varied with the sample type and probe position to yield similar energy deposition and thus similar surface temperature. To electrically isolate these tubes from the water system, the open end of the sample was joined to one end of a dumb-bell shaped ceramic insulator (machined from alumina) by means of a compression seal. The other end of the ceramic insulator was joined to a stainless steel 304L flange by means of another compression seal. The flange provided a means for welding the probe assembly into a water manifold. Electrical contact to the sample was made via a nickel wire which was spot welded to the inside of the probe prior to joining. This wire was fed through a hole in the ceramic. Samples were fabricated from stainless steel 304L, alloy 718, and tantalum. Only the results from alloy 718 are reported here. Inconel 718 is a crucial material, used to construct the window between UHV and the target chamber as well as to clad the tungsten (W) targets for the spallation source. Although the ceramic sealing process required the corrosion samples to be held at approximately 800-900^{o} C for 10 to 20 minutes, similar heat treatment of alloy 718 in the lab showed no substantial microstructural differences when compared to the as received material.

The water manifold held 3 seperate experiments (Figure 3). The in-beam experiments consisted of 7 tubes arranged in a close-packed array (Fig. 3 bottom). Each tube contained a corrosion sample. The manifold was welded to the bottom of an 11’ supporting insert which supported the weight of the manifold and provided the necessary conduits for electrical and water connections. Similar corrosion probes to examine SCC and the effects neutrons on corrosion rate were also attached to the bottom of this insert . Thermocouples (TC's) attached to the front of the manifold verified the position, size and shape of the proton beam while additional TC's brazed to the outside of each tube were used to calculate the surface temperature of the corrosion samples. A diagram depicting the corrosion insert and its relative position at the target station is presented in Figure 4 (insert 17B). All experimental in-beam data presented here were collected with only the corrosion insert in place; that is, inserts 17A and 18A through 18C were raised to a height sufficient to remove them from the proton beam path.

In addition to the in-beam probes, samples were also located out-of-beam, downstream from the manifold (Figure 1). Out-of-beam corrosion samples were fabricated from Al6061, Al5052, W, Ta, 304L, 316LN, and alloy 718 (only the results of alloy 718 are reported here). The probes which held these samples were purchased from a commercial vender "off-the-shelf." They employed glass to metal seals. The system also contained a number of additional probes to monitor OCP, water conductivity, and hydrogen concentration.

After assembling the water system, it was steam cleaned, rinsed with a 50/50 mixture of ethanol and deionized (DI) water followed by several rinses with DI water alone. Following this cleaning procedure the system was filled with DI water. A mixture of Ar-6%H_2 was continuously bubbled into the water system such that the dissolved hydrogen concentration was approximately 0.30 ppm. This hydrogen concentration was maintained during the course of the experiments.

Because the cooling water in the LANSCE A6 corrosion loop was deionized prior to being pumped into the system and had an initial resistivity of approximately 10^6 ohm˙cm, electrochemical impedance spectroscopy (EIS) was used to measure corrosion rate. Traditional dc electrochemical techniques for measuring corrosion rate contain an error due to the geometric solution resistance (i.e., $V_{applied}/I_{meas} = R_{meas} = R_{sol}+R_{pol}$. where R_{pol} is the polarization resistance and is inversely proportional to corrosion rate, R_{sol} is the geometric solution resistance, and R_{meas} is the measured resistance). Typically R_{sol} is several orders of magnitude smaller than R_{pol} and is, therefore, often neglected. Because R_{sol} in the LANSCE A6 water loop was large relative to R_{pol}, the uncorrected polarization resistance would have been over estimated and, as a result, the corrosion rate would have been be underestimated. While there are methods in traditional dc electrochemistry to compensate for R_{sol} indirectly (such as current interrupt), EIS is a powerful non-destructive ac technique that allows R_{sol} to be measured directly in each experiment(20, 21, 22). Here, EIS measurements were conducted with a 30 mV sinusoidal voltage perturbation over the frequency range of 0.003 - 1 kHz. No applied dc potential was employed; that is, all measurements were conducted at the OCP. To eliminate the effects of ground loops, floating ground EIS systems were used.

Real-time Electrochemical Measurements During Proton Irradiation

OCP data as a function of time before and during proton irradiation for the in-beam and out-of-beam 718 samples are presented in Figure 5. While the OCP of the out-of-beam sample remained constant independent of irradiation, when the proton beam was turned on to a beam current of 100 nA at 230 seconds, a sharp positive shift in the in beam OCP from its steady state value of -0.03 V vs ground to a value of 0.07 V SCE was observed. Similarly, upon turning the beam off a sharp decrease in the OCP was always observed (not shown). The sharp positive increase in the OCP after turning the beam on is consistent with an increase in the concentration of total oxidant at the in-beam probe / solution / beam spot interface while the lack of change in the OCP the out-of-beam sample when the beam was turned on is evidence that no increase in the bulk concentration of total oxidant occurred. Moreover, had the concentration of total oxidant in the bulk solution increased, the sharp decrease in the OCP of the in-beam probe when the beam was turned off would not have occurred.

Typical EIS data from the in-beam 718 probe as a function of beam current are presented in the form of Bode magnitude and phase plots in Figure 6. The data in Figure 6 were modeled by the electrical equivalent circuit presented in Figure 7. This circuit is known as a simplified Randles circuit(23). By subtracting R_{sol} from the low frequency impedance (equal to $R_{sol}+R_{pol}$), R_{pol} for the sample was determined. Data modeling was accomplished by using a complex non-linear least squares fit (CNLS) of the data. A typical CNLS fit for the in-beam 718 probe at a beam current of 400 μA is presented in Figure 8. From the polarization resistance, corrosion rate was determined from the well know expressions:

$$i_{corr} = 0.026 / R_{pol} \qquad \text{Eq. 1}$$

$$CR_{mpy} = \frac{129(i_{corr} EW)}{D} \qquad \text{Eq. 2}$$

where i_{corr} is the corrosion current density in milliamps/cm^2, R_{pol} is the *area normalized* polarization resistance in ohm·cm^2, EW is the equivalent weight in g/equivalent., D is density in g/cm^3, and CR is corrosion rate in mils/yr. Equation 1 assumes the anodic and cathodic Tafel slopes are equal to 0.12 V. The error associated with assumption is typically within than the range of -38.5% to + 22.1%(24).

The effect of beam current on the corrosion rate of the in-beam 718 probe is presented in Figure 9. The exponential increase in corrosion rate of the in-beam sample is consistent with an increase in concentration of total oxidant in the diffusion boundary layer. In comparison, the corrosion rates for the out-of-beam 718 sample (supply side) were orders of magnitude less than the in-beam corrosion rates (Figure 10). Moreover, no correlation between the corrosion rate of the out-of-beam-sample and beam current or solution resistivity was observed. As noted above, R_{pol} is the *area normalized* polarization resistance in ohm·cm^2, therefore, these corrosion rates assume uniform corrosion current density across the entire surface. For the out-of-beam samples this assumption is valid in the absence of pitting corrosion. For the in-beam samples, these rates are likely non-conservative as the Gaussian beam profile irradiated only a small fraction of the sample surface (10-20%). It has been shown for tungsten targets that the corrosion rate is highest at the center of the beam spot(25). Currently we are developing a method to use the Gaussian beam profile to normalize R_{pol} as a function of position across the sample. It is hoped that this will provide an upper boundary for the maximum corrosion rate that may be occurring at the center of the beam spot. A complete discussion of this analysis will appear in later publications.

The OCP of the out-of-beam sample was observed to increase during the course of the irradiation period (Figure 11). This observation was consistent with an increase in concentration of total oxidant in the water system. As determined by iodometric titration (a technique sometimes called Kingzettís method), the final concentration of H_2O_2 in the water system at the end of the 107 day irradiation period was 3.3×10^{-4} M. The effect of 3×10^{-4} M H_2O_2 on the potentiodynamic polarization curve of 718 (in boric acid / sodium borate buffer, pH 7.2) is seen in Figure 12.

While the OCP of the sample in H_2O_2 is approximately 175 mV more positive in the peroxide solution, the difference in i_{corr} is almost imperceptible: $2.9x10^{-8}$ A/cm^2 vs. $2.4x10^{-8}$ A/cm^2 with and without peroxide respectively. Recall that i_{corr} is directly proportional to corrosion rate (Eq. 2). In addition, the cathodic reaction rate is higher in the presence of H_2O_2 for any given potential which is reflective of peroxides role as an oxidant. However, no large increase in the corrosion current density for 718 was observed in the peroxide solution as might be anticipated for a material that exhibits passivity over a wide potential range. From these results we conclude that the small increase in the concentration of total oxidant observed in the LANSCE A6 water system due to radiolysis was responsible for observed increase in the OCP of the out-of-beam 718 sample with time. Moreover, the presence of peroxide is not necessarily associated with an increase in corrosion rate which explains the relatively constant out-of-beam 718 corrosion rates.

While the results presented in this paper have been interpreted in terms of a water radiolysis mechanism, spallation of the passive film and temperature increases (due to energy deposition from the proton beam) may also increase corrosion rates at the OCP. Currently we are examining the effect of temperature in the laboratory to eliminate this unknown. To address the possibility of oxide spallation (due to low energy spallation products not high energy protons) we are using surface enhanced Raman spectroscopy to characterize the passive film during irradiation. Additional studies will use cyclic voltammetry to measure peroxide concentration differences between the double layer and bulk solution.

Acknowledgments

All work on this project was completed under the auspices of the University of California for the US DOE contract #W-7405-ENG-36. The authors gratefully acknowledge: the support of Laurie Waters and the APT Project Office; the hands-on work of Donald Pile; helpful discussions with Luke Daemen, Walt Sommer, Stuart Maloy, Gordon Willcutt, and the APT Materials Steering Committee; the engineering expertise of Richard Werbeck, Bob Brown, Eugene Zimmerman, and countless others at LANSCE. We would also like to thank Len Reed and Paul Lavoi of Inta Corp in Santa Clara CA for designing the in-beam corrosion probes.

About the Authors

Scott Lillard earned his PhD. in Materials Science and Engineering from The Johns Hopkins University in 1992. He pursued his post-doctoral education at the University of Virginia, Center for Electrochemical Sciences and Engineering. He is currently a technical staff member at the Los Alamos National Laboratory, Materials Corrosion and Environmental Effects Lab.

Darryl P. Butt earned his Ph.D in Ceramic Science in 1991 and his B.S. in Ceramic Science & Engineering from Penn State University, Materials Research Institute. He is currently a technical staff member at the Los Alamos National Laboratory, Non-Proliferation and International Security Division.

For more information , contact R.S. Lillard, MS G755, Los Alamos National Laboratory, Los Alamos, NM, 87545; (505) 667-6325, fax (505 667-2264; email lillard@lanl.gov; http://macrsl.mst.lanl.gov/MCEL.html.

References

1. W. G. Burns, P. B. Moore, *Radiation Effects,* **30** (1976), pp. 233-242.

2. W. G. Burns, W. R. Marsh, *Journal of the Chemical Society, Faraday Transactions 1,* **77** (1981), pp. 197-215.

3. H. Christensen, *Nuclear Technology*, **109** (1994), pp. 373-382.

4. C. D. Jonah, D. M. Bartels, A. C. Chernovitz, *Radiation Physics and Chemistry,* **34** (1989), pp. 145-156.

5. S. R. Lukac, *Radiation Physical Chemistry,* **33** (1989), pp. 223-230.

6. S. M. Pimblott, J. A. LaVerne, *Radiation Research,* **129** (1992), pp. 265-271.

7. M. E. Indig, J. E. Weber, *Corrosion/83*, (Houston, TX: NACE, 1983), paper# 124.

8. W. R. Kassen, R. P. Jones, J. L. Tollefson, *Corrosion/92*, (Houston, TX: NACE, 1992), paper# 112.

9. M. J. Fox, "A Review of Boiling Water Reactor Chemistry: Science, Technology, and Performance" *NUREG/CR-5115 ANL-88-42* (Argonne National Laboratory for the US Nuclear Regulatory Commision, 1989).

10. C. C. Lin, R. L. Cowan, R. S. Pathania, *Corrosion/93,* (Houston, TX: NACE, 1993), paper# 619.

11. L. G. Ljungberg, D. Cubicciotti, M. Trolle, *Corrosion/85*, (Houston, TX: NACE, 1985), paper# 100.

12. Y. J. Kim, *Corrosion/96*, (Houston, TX: NACE, 1996), paper# 102.

13. M. Simnad, R. Smoluchowski, *Physics Review,* **98** (1955), pp. 1891-1892.

14. M. Simnad, R. Smoluchowski, *Physics Review*, **99** (1955), pp. 1961-1962.

15. R. S. Glass, G. E. Overturf, R. A. v. Konynenburg, R. D. McCright, *Corrosion Science,* **26** (1986), pp. 577-590.

16. L. Darong, *Journal of Chinese Society of Corrosion and Protection,* **1** (1981), pp. 37-47.

17. Y. J. Kim, R. A. Oriani, *Corrosion*, **43** (1987), pp. 85-91.

18. Y. J. Kim, R. A. Oriani, *Corrosion*, **43** (1987), pp. 92-97.

19. R. S. Lillard, D. P. Butt, *submitted to Materials Characterization*, (1998).

20. I. Epelboin, C. Gabrielli, M. Keddam, H. Takentouti, in *Electrochemical Corrosion Testing, ASTM STP 727* , F. Mansfeld, U. Bertocci, eds., (Baltimore : ASTM, 1981), pp. 150-166.

21. D. D. MacDonald, M. C. H. Mckubre, in *Electrochemical Corrosion Testing, ASTM STP 727* , F. Mansfeld, U. Bertocci, eds., (Baltimore : ASTM, 1981), pp. 110-159.

22. J. R. Macdonald, *Impedance Spectroscopy*, (New York: Wiley Publishing, 1987).

23. J. E. B. Randles, *Discussions of the Faraday Society*, **1** (1947), pp. 11-19.

24. F. Mansfeld, in *Electrochemical Techniques for Corrosion Engineers* , R. Baboian, ed., (Houston, TX : NACE, 1986), pp. 67-71.

25. S. Maloy, W. Sommer, D. Butt, S. Lillard, *unpublished data*.

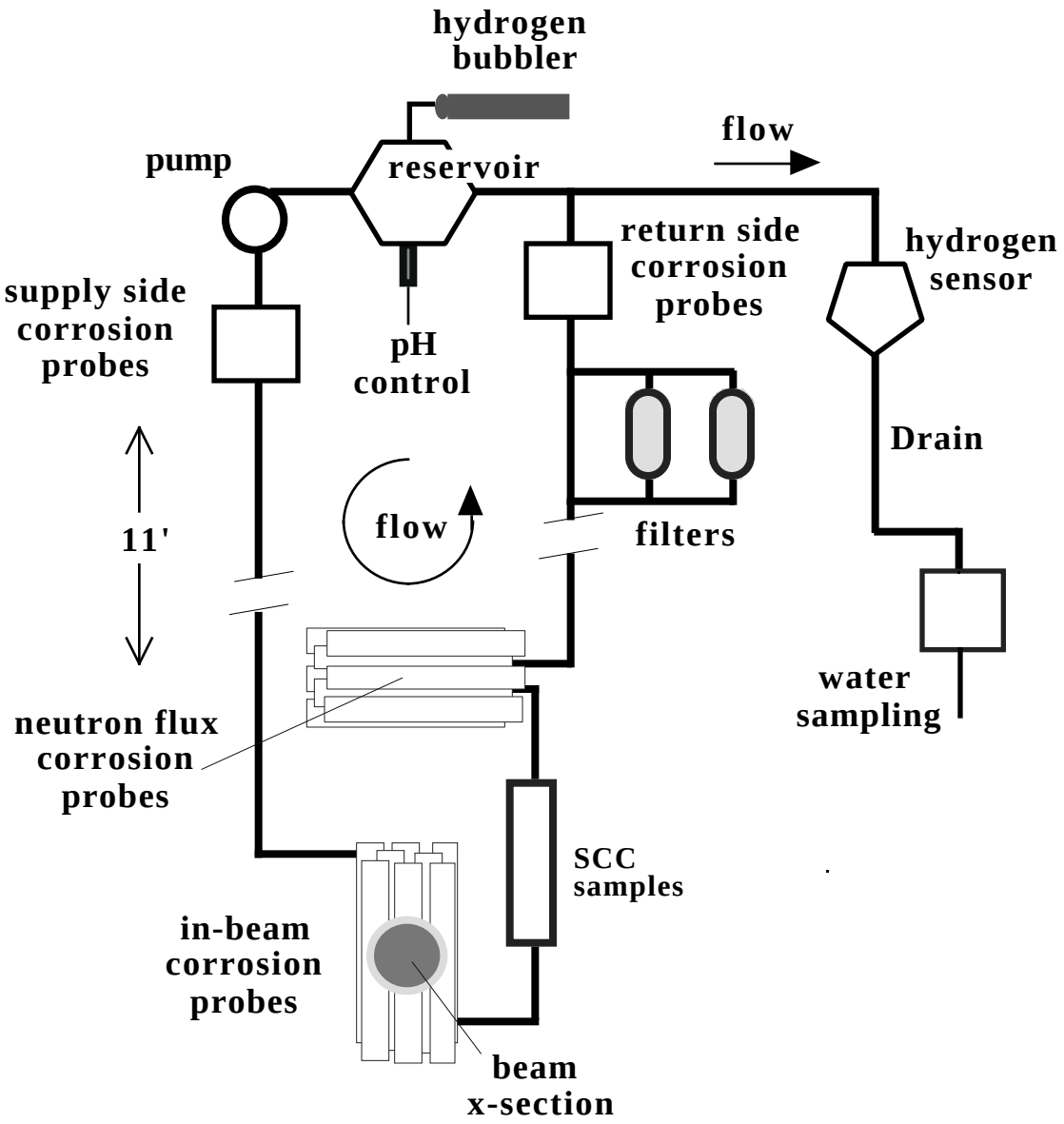

Figure 1 A diagram representing the corrosion water system at the LANSCE A6 Target Station. This system was used to measure the real-time corrosion rates of materials during proton irradiation.

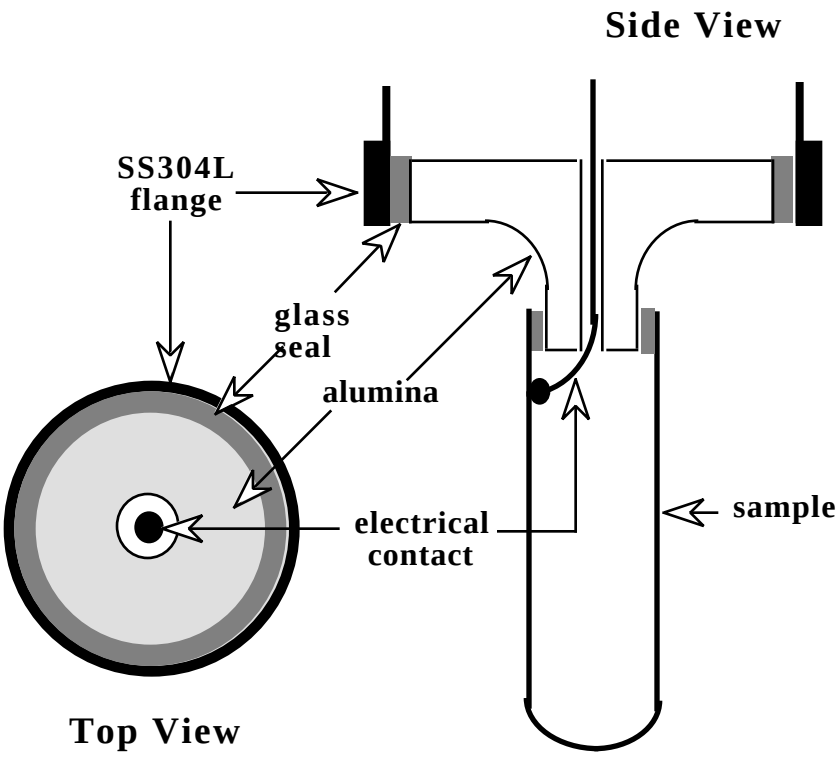

Figure 2 A diagram depicting the corrosion probes used to electrically isolate the corrosion samples from the water system. Samples were mounted on the alumina by means of a compression seal

Figure 3 A photograph of the corrosion insert (17B) prior to being set in place at the A6 Target Station. Photo is from the rear of the insert, that is, the proton beam is perpendicular to the page and would strike the in-beam probes from the opposite side.

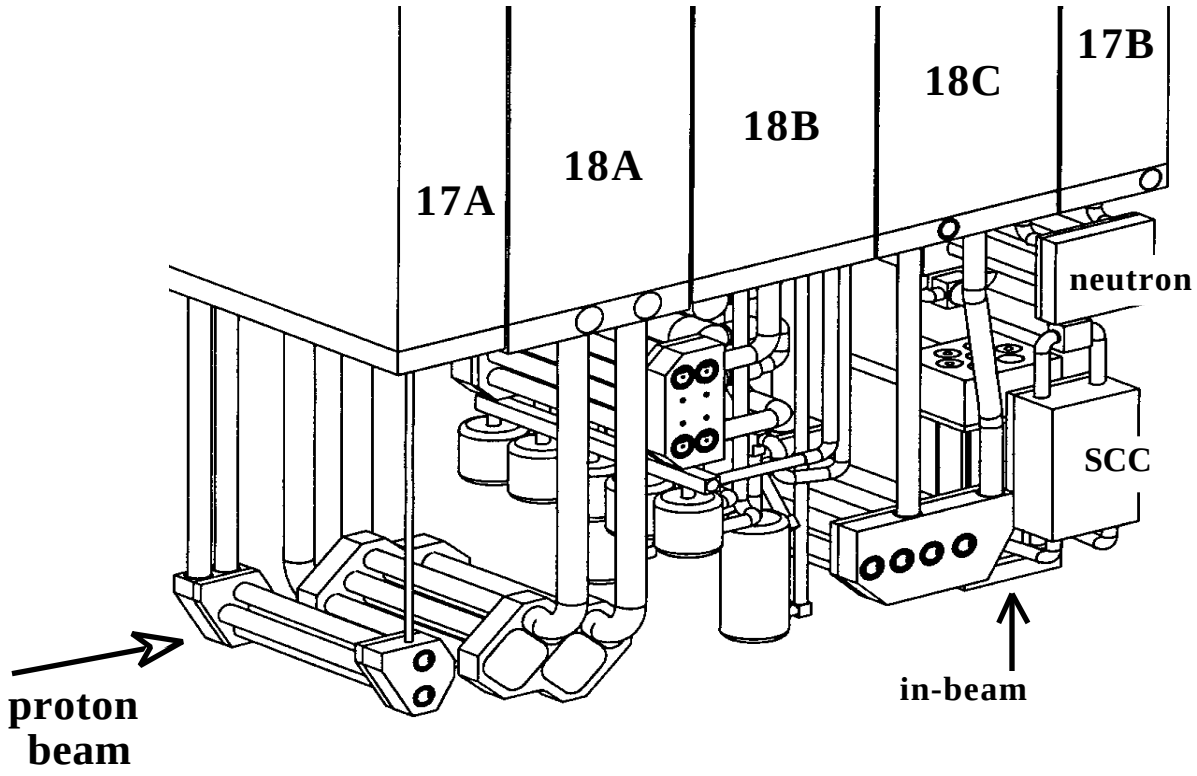

Figure 4 A diagram representing the A6 Target Station at LANSCE and all of the materials irradiation inserts. All in-beam data reported on in this paper were collected with inserts 17A-18C removed from the beam path.

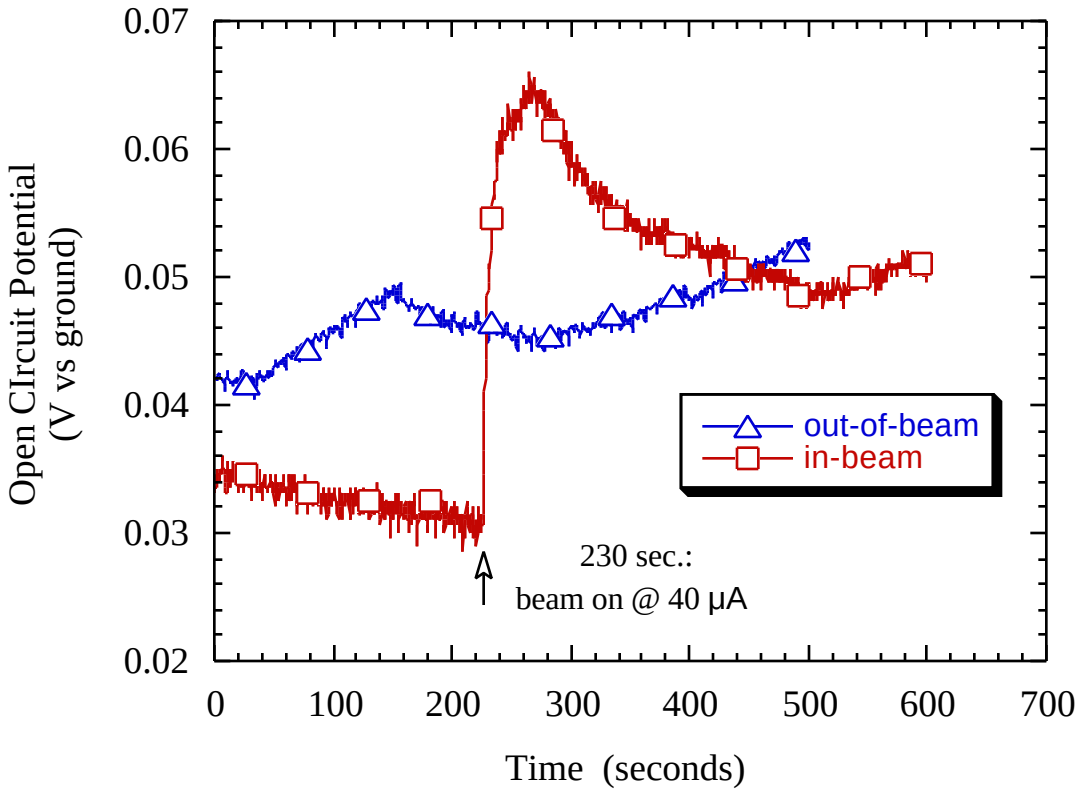

Figure 5 Open circuit potential of the in-beam and out-of-beam alloy 718 samples before and during proton irradiation. Potential was measured with respect to ground (that is, the stainless steel water system).

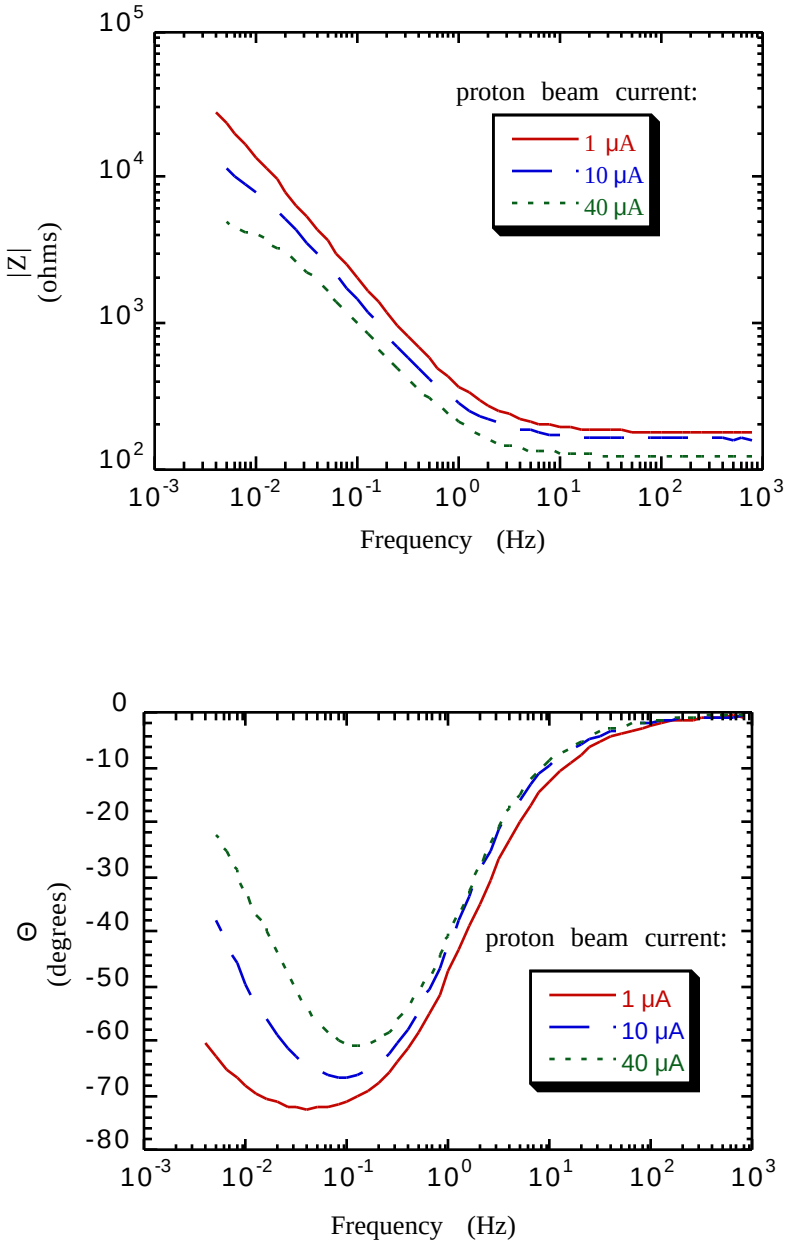

Figure 6 Bode magnitude (**a**) and phase (**b**) plots from the 718 sample during proton irradiation at proton beam currents of 1, 10, and 40 μA.

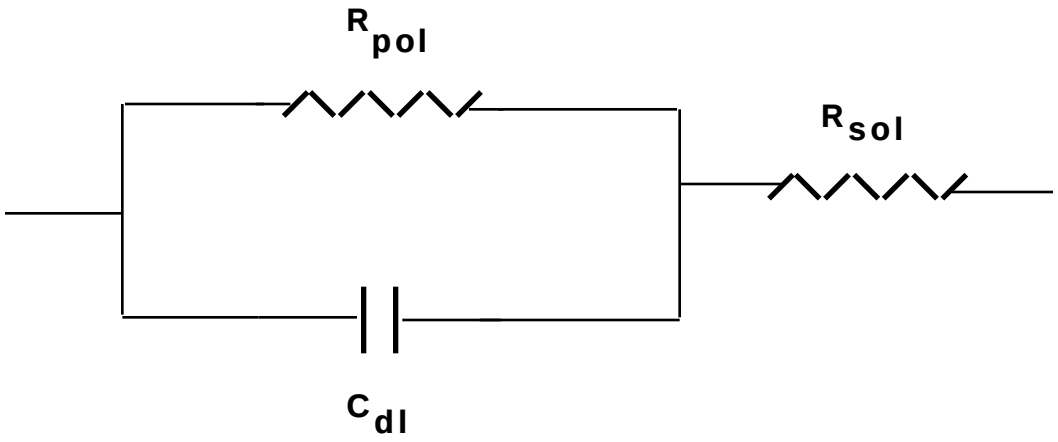

Figure 7 Equivalent circuit model used in complex non-linear least squares fitting of the EIS data where: R_{pol} represents the polarization resistance and is inversely proportional to corrosion rate, C_{dl} represents the double layer capacitance, and R_{sol} represents the geometric solution resistance.

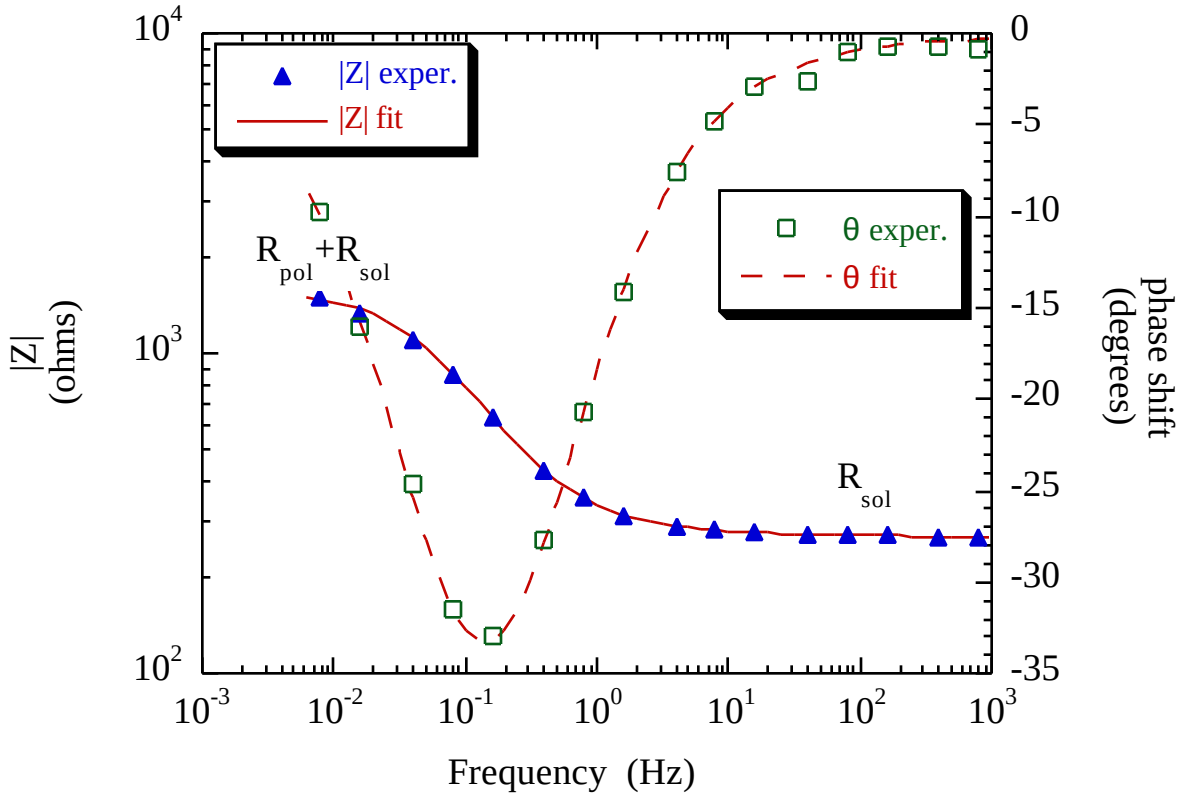

Figure 8 Bode magnitude and phase data from the in-beam 718 sample during radiation at 400 μA and the CNLS fit of the data to the equivalent circuit shown in Figure 7. For clarity, not all experimental data are shown .

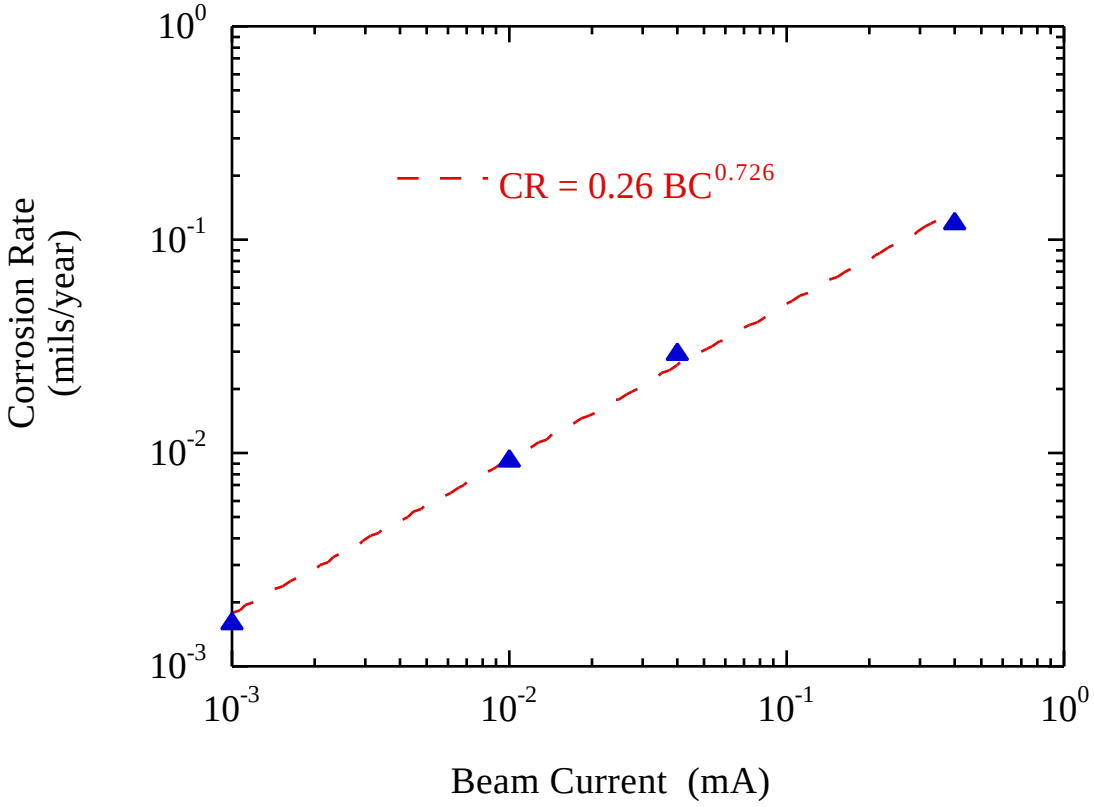

Figure 9 Corrosion rate from the in-beam 718 sample as a function of proton beam current. The calculation of corrosion rate used the total surface area making these rates non-conservative as the beam spot covered less than 30 % of the sample surface.

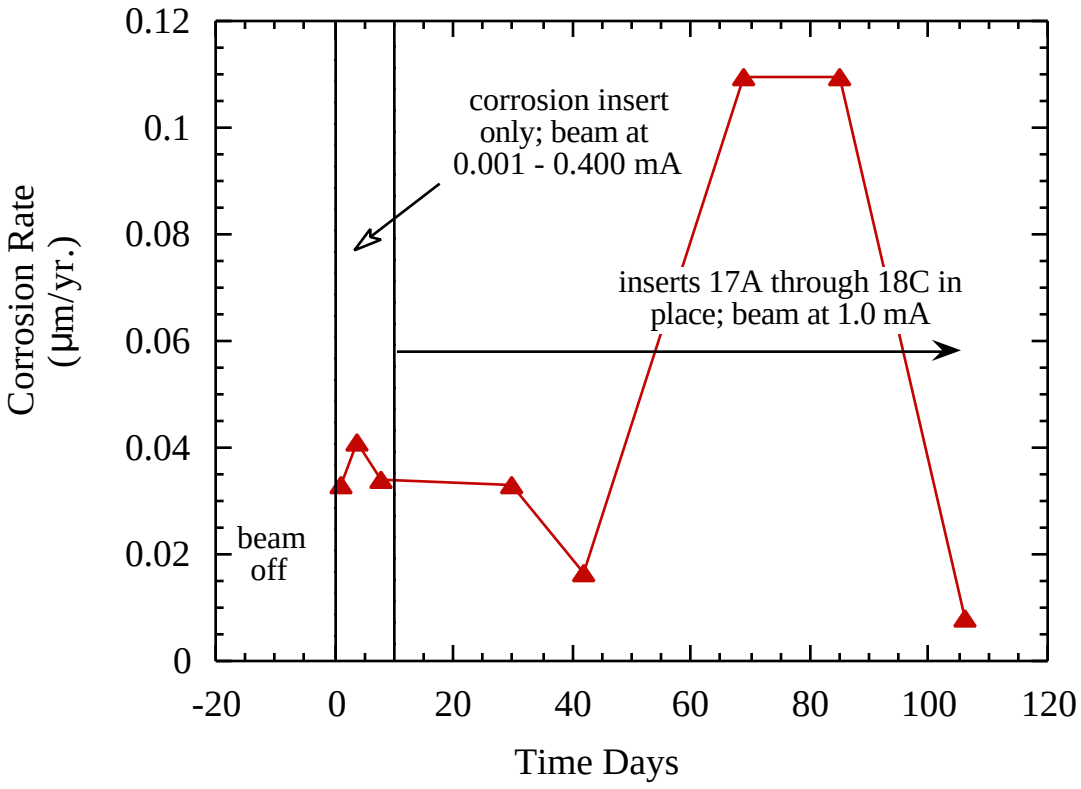

Figure 10 Corrosion rate from the out-of-beam 718 sample as a function of irradiation time. The first 10 days of data were collected with all other inserts removed from the beam path. During the remainder of the irradiation all inserts were in place. (1 mil = 0.001")

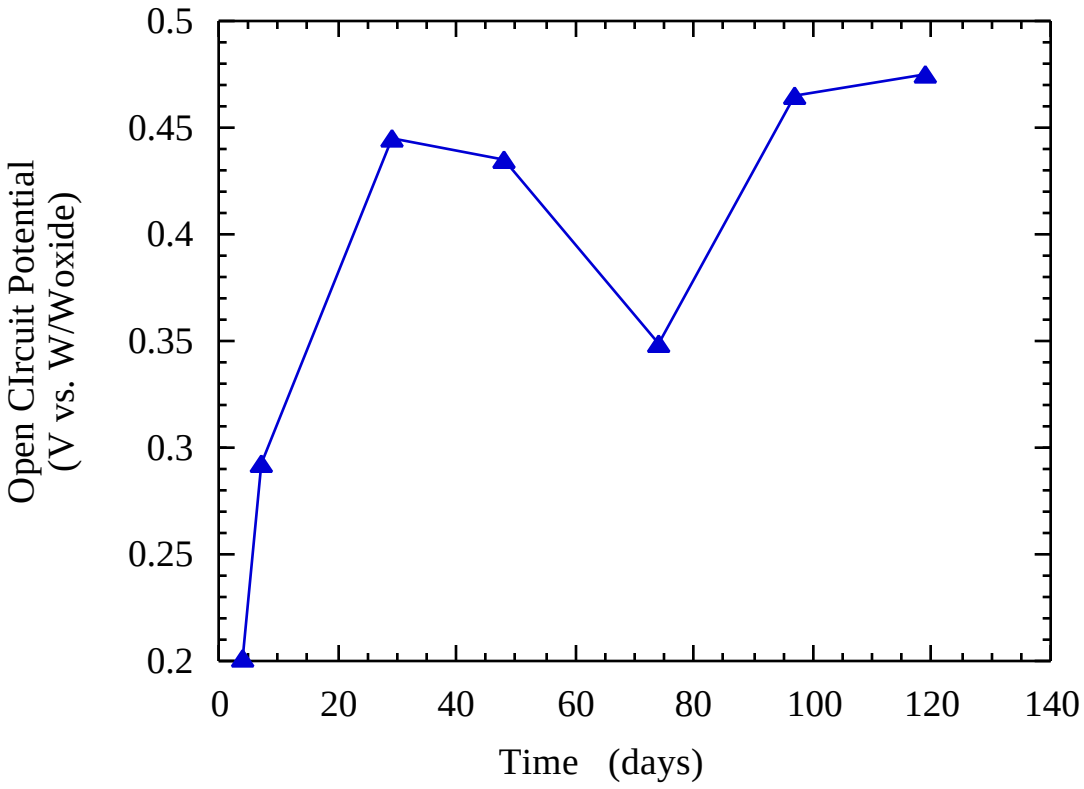

Figure 11 Open circuit potential of the out-of-beam 718 sample as a function of irradiation time. The potential was measure with respect to a tungsten / tungsten-oxide electrode (approximately -0.21V vs. NHE).

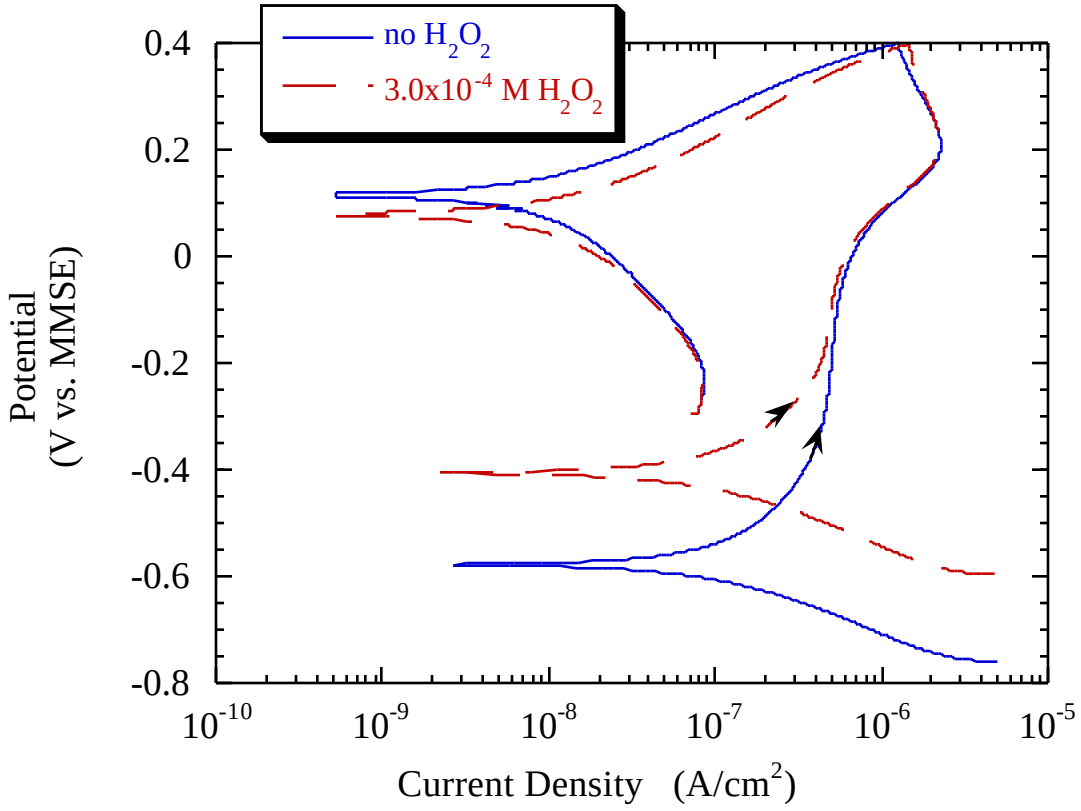

Figure 12 Potentiodynamic polarization curves for alloy 718 in borate buffer pH 7.2 with and without the addition of hydrogen peroxide. While peroxide increased the OCP by approximately 0.20 V, the small increase in corrosion current density is almost imperceptible. (Arrows indicate scan direction)